REVIEW Neuro

Dynamic Susceptibility Contrast MRI in Gliomas: What the Radiologist Needs to Know

Sameeha Fallatah[1,2], Xavier Golay[1], Rolf Jäger[1,2], Sotirios Bisdas[1,2]

[1] *Department of Brain Repair and Rehabilitation, Institute of Neurology, University College London, UK*

[2] *Department of Neuroradiology, The National Hospital for Neurology and Neurosurgery, UCL Hospitals NHS Trust, London, UK*

SUBMISSION: 27/06/2016 | ACCEPTANCE: 19/09/2016

ABSTRACT

Perfusion MRI analyses tissues' temporal responses to the inflowing exogenous contrast agents or labeled blood to characterize the hemodynamics properties of the tissues. Perfusion MRI techniques are sensitive to microvasculature, thus, can be a robust tool to study brain tumors where the neovascularization is a hallmark of malignancy. The derived indices can be helpful in many aspects, including tumor grading, prediction of malignant transformation, patient management planning, and monitoring treatment responses. A major MRI perfusion approach using exogenous contrast agent is dynamic susceptibility contrast MRI (DSC-MRI). With the increasing need for perfusion MR imaging in clinical practice, it is important to understand the basic principles of the technique and its meaningful clinical applications. In this review, we discuss the most commonly used perfusion sequence, DSC-MRI. We provide a comprehensive overview of the principles for clinical neuroradiologists and neuroscientists to help improve their understanding of the underlying theory and the technical aspects of DSC-MRI, as well as image acquisition, image analysis, its possible pitfalls, and its clinical applications in tumor imaging.

KEY WORDS: perfusion MRI; dynamic susceptibility contrast; gliomas; cerebral blood flow; cerebral blood volume

1. Introduction

Cerebral perfusion refers to the steady state delivery of oxygen and nutrients via blood to brain tissue per unit volume or mass. It is typically measured in milliliters per 100 grams of tissue per minute (ml/100g/min) [1-3]. Normal perfusion requires sufficient cardiac output and healthy blood vessels [1]. The term 'perfusion' strictly means -in physiology- blood flow at the capillary level [1]. However, it is often broadly applied to include other hemodynamic parameters, such as cerebral

CORRESPONDING AUTHOR, GUARANTOR

Sotirios Bisdas, MD, Ph.D, M.Sc (Advanced Oncology), FESHNR
Department of Neuroradiology, The National Hospital for Neurology and Neurosurgery, 8-11 Queen Square, London WC1N 3BG, United Kingdom
E-mail: s.bisdas@ucl.ac.uk

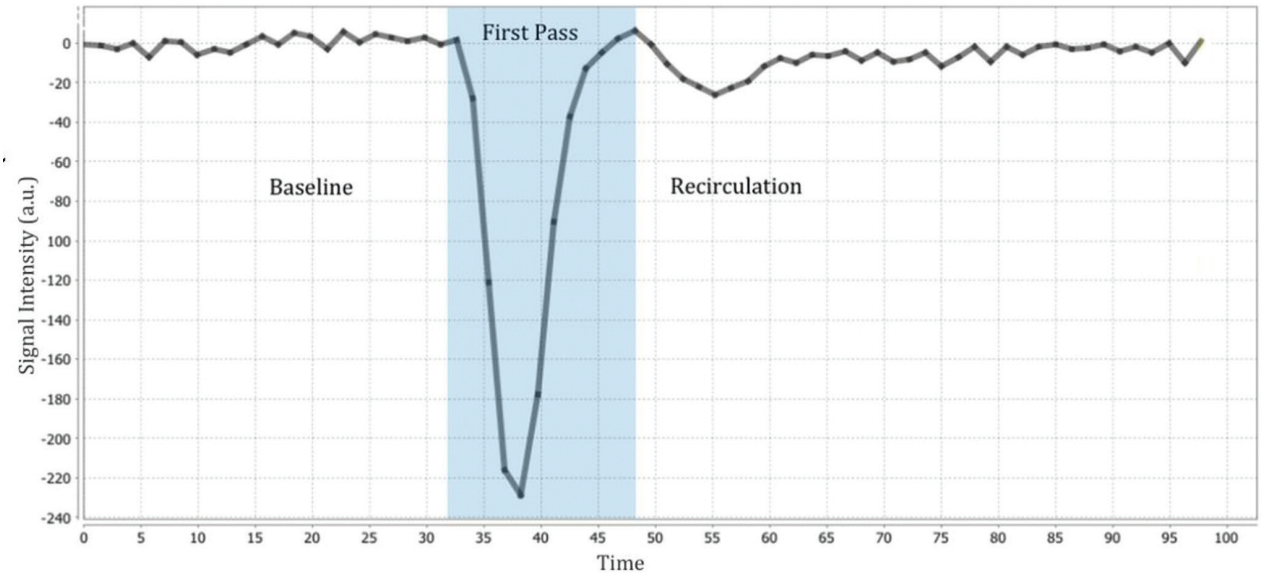

Fig. 1: *The graph demonstrates the changes in signal intensity over time after a bolus of contrast agent injection*

blood volume (CBV), mean transit time (MTT), and vascular permeability parameters such as the forward transfer constant (K^{trans}) and the fractional volume of the extravascular extracellular space (ve) [4]. Blood flow along major arteries and veins is not "perfusion" and measured in unit mass or volume per unit time, e.g. mL/s [5]. Brain parenchyma survival depends on an adequate blood supply, and thus hypoperfusion (such as in stroke) and hyperperfusion (such as in epilepsy and tumors) threatens the viability of the brain tissue. Perfusion indices have been used as imaging biomarkers in many diseases, such as stroke [6-11], tumors [12-18], epilepsy [19-22], neuroinflammatory and neurodegenerative disease [23-28].

DSC-MRI benefits from signal changes, which accompany the passage of a gadolinium-based contrast agent (GBCA) through the cerebrovascular system, to quantify perfusion. It is the most often used technique to assess noninvasively the tumor vascular density which is directly related to the tumor grade in glioma. It has shown great potential in brain tumor imaging. The derived parameters are relative CBV, CBF and MTT (rCBV, rCBF and MTT). rCBV, in particular, is the most reliable parameter for characterization of brain tumors, MTT is the least [29]. DSC-MRI has become increasingly important not only in diagnosis and management planning of glioma but also in assessing treatment response [30-33]. The increased use of DSC-MRI necessitates having a solid understanding of the techniques. In this review, we discuss DSC-MRI methods including physical principles and quantification techniques, protocols and parameters, pitfalls and limitations, clinical applications in brain tumors and future endeavors in this field.

2. Fundamental Concepts

DSC-MRI acquisition: DSC-MRI relies on a bolus injection of a paramagnetic contrast agent coupled with rapid measurement of T2/T2* signal change during the first passage of the bolus through the cerebral circulation [34,35]. In DSC-MRI, images are acquired before, during, and after contrast agent injection while the signal intensity changes are measured over time. The detailed physical principles and DSC-MRI data quantification are beyond the scope of this review and can be found in [36-40]. Here, we are only going to emphasize the most important concepts.

Origin of Signal: The intravascular compartmentalization of GBCA produces a local magnetic field inhomogeneity that disturbs the nearby spins and induces a transient decrease in signal intensity called "*Susceptibility Contrast*". The susceptibility contrast is most marked on T_2* (gradient echo) and less on T_2 (spin echo)-weighted sequences. The drop in the signal is proportional to the tissue vascularity and the contrast agent concentration. The signal intensity in DSC-MRI has arbitrary units and reflects the hemodynamics of the contrast agent within a tissue voxel.

Signal intensity-time curve: The changes in MR signal intensity over time are divided into three stages: The baseline, the first passage of the bolus, and the recirculation period [41], **Fig. 1.** Firstly, *the baseline* is the period where images are acquired before the arrival of the contrast agent bolus, the signal intensity is, therefore, assumed to be constant. Secondly, GBCA injection is followed by a period of a transient rapid signal drop called *the first passage of the bolus*, the maximum signal drop corresponds to the time of maximum contrast concentration. After reaching the minimum signal (or maximum contrast concentration), signal intensity starts to return to the baseline value. The first passage is often partially overlapped with *the recirculation period*, which causes a smaller and slower secondary signal drop. The recirculation period results from re-entering of the contrast agent. Finally, tissue signal theoretically recovers to the baseline.

Conversion of signal intensity to concentration: The signal change over time S(t) is converted into ΔR2*(t). ΔR2*, which is the transversal relaxation rate, is assumed to be linearly proportional to contrast concentration, equation [1]:

$$C(t) = k \cdot \Delta R2^*(t) \qquad \text{(Equation 1)}$$

$$\Delta R2^*(t) = -\frac{1}{TE} ln\left(\frac{S(t)}{S0}\right) \qquad \text{(Equation 2)}$$

$$C(t) = -\frac{k}{TE} \cdot ln\left(\frac{S(t)}{S0}\right) \qquad \text{(Equation 3)}$$

R2* and T2* are the transversal relaxation rate and time, C(t) is the contrast concentration at time t, S(t) and S0 are the signal intensity at time t and the baseline respectively, TE is the echo time of the MR sequence, k is a proportionality constant that depends on the contrast agent, pulse sequence, field strength, blood volume and vascular morphology. Therefore, if we assume negligible T1 effect during the first bolus passage, C(t) can be calculated from the signal intensity changes with respect to its baseline value, equation [3].

CBV quantification: DSC-MRI quantification is based on the theory of tracer kinetics for intravascular non-diffusible tracers [42,43] i.e. GBCA remains intravascular during its first passage through the brain [41,44]. It assumes that the dominant contrast is T2 weighted and T1 effect is negligible. It also assumes that GBCA tissue concentration is linearly proportional to the rate of the signal change. Based on these assumptions and by applying traditional tracer kinetic models for intravascular agents, CBV can be obtained by integrating the area under the concentration-time curve, equation [4]. However, absolute perfusion measurements require the determination of the arterial input function (AIF) and subsequent deconvolution analysis.

$$CBV = \frac{H_f}{\rho} \frac{\int_0^t Ct\,(t)dt}{\int_0^t Ca\,(t)dt} \qquad \text{(Equation 4)}$$

Where ρ is the tissue density, H is the haematocrit level and $Hf=(1-H_{artery})/(1-H_{capillary})$. $C_t(t)$ and $C_a(t)$ represents the concentration of the contrast in the tissue and a large artery at time t.

Arterial input function (AIF): AIF is the concentration of GBCA passing through an artery feeding the brain or a tissue of interest. AIF is used to calibrate the perfusion measurements by defining the shape of the actual bolus before entering the cerebral microvasculature [45]. The AIF is typically measured on voxels found within, or near an artery as an approximately linear relationship between the tissue relaxivity and GBCA concentration is found in a voxel adjacent but not within the artery [46].

By applying the indicator dilution theory, the tissue concentration, $C_t(t)$, can be modeled as the mathematical convolution between AIF ($C_a(t)$) and the fraction of the bolus of contrast agent remaining in the tissue at time t following the arrival of an ideal instantaneous bolus, known as the tissue residue function, R(t):

$$Ct(t) = \alpha \cdot CBF \cdot Ca(t) \otimes R(t) = CBF \cdot \int^t Ca\,(\tau)R(t-\tau)d\tau$$

(Equation 5)

Where α is the proportionality constant ($\alpha=\rho/Hf$), the symbol $\otimes$ represents convolution, $R(t-\tau)$ is the tissue residue function at time t, following the ideal bolus injection at time τ [41].

Deconvolution analysis: The deconvolution is a mathematical step by which the contribution of the AIF is removed from the tissue to estimate the residue function. The residue function (R) is the fraction of tracer still present in the tissue after an ideal instantaneous bolus injection into the tissue-feeding vessel at the entrance of the capillary network at time 0. CBF quantification requires deconvolution of the AIF ($C_a(t)$) and the measured

contrast agent concentration-time curve $C_t(t)$, as shown in equation [6]. The most commonly used method is the singular value decomposition (SVD) [47].

$$\alpha \cdot CBF \cdot R(t) = C_t(t) \otimes^{-1} C_a(t) \quad \text{(Equation 6)}$$

Where $\otimes^{-1}$ represents the deconvolution operator.

Mean transit time MTT, which represents the average time for a molecule of contrast agent to pass through the tissue vasculature following an ideal bolus injection, can be calculated using the central volume theorem as [36].

$$\mathrm{MTT} = \int_0^t \mathrm{t\,h}(\tau)\mathrm{d}\tau = \frac{\mathrm{CBV}}{\mathrm{CBF}} \quad \text{(Equation 7)}$$

Where h(τ) is the transport function at time τ, which is defined as the impulse response function of the particles exiting the tissue [48].

The scaling factor of the residue function is equal to CBF while CBV is the area under the residue function and MTT is calculated as the ratio of CBV/CBF [4]. The abbreviations rCBV, rCBF, and rMTT refer to "regional" or "relative" CBV, CBF, and MTT, the later indicating relative and not absolute measurements of these parameters [49].

Absolute versus relative perfusion metrics: Relative CBV (rCBV) generally, refers to a qualitative measure obtained without consideration of the AIF. However, perfusion measurements in its absolute units (ml/100g/min for CBF and ml/100g/min for CBV) are nearly impossible in a clinical setting. Absolute quantification requires the knowledge of proportionality constants that intervene in the conversion of the signal into concentration time curves. These constants depend on multiple factors such as the MRI scanner, the contrast agent and the acquisition parameters as well as the exact hematocrit level and tissue density, which may vary in health and disease. Furthermore, absolute quantification is hampered by partial volume effects and other problems related to AIF selection. Thus, perfusion measurements always remain relative to the methods used. rCBV ratio, on the other hand, is a measurement obtained relative to the contralateral normal brain, typically, the normal appearing white matter, it is sometimes called normalized rCBV (nrCBV).

3. DSC-MRI Protocol

DSC-MRI Sequence: DSC-MRI is based on a fast multi-slice imaging sequence, with two-dimensional (2D) or three-dimensional (3D) dynamic acquisition with sufficient temporal resolution [50-53] to catch the transient MR signal drop which lasts approximately for 10 seconds with sufficient temporal resolution [50-53]. Echo planar imaging (EPI) is the imaging technique of choice with either T2*-weighted gradient-echo (GE) or T2-weighted spin-echo (SE) pulse sequences. EPI techniques provide whole-brain coverage with reasonable signal-to-noise ratios (SNRs) [54]. GE-EPI is often used, clinically, because it is faster. Thus, it gives better coverage of the brain with the same given repetition time because it has shorter TE than SE-EPI. Moreover, it is more sensitive to magnetic susceptibility effects since it does not involve the use of a refocusing pulse. Typically the GBCA dose used is only half of that used for SE-EPI, and also, it exhibits higher SNR. GE-EPI images are sensitive to a wide range of vessel sizes with greater sensitivity to macrovasculature. SE-EPI has the inherent sensitivity to perfusion at microvascular level, with vessel size less than 8 μm [55,56].

Echo time (TE): For a GE sequence, the optimal signal drop is achieved by setting the MR TE equal to T_2^* of the tissue [57]. Long TEs decreases T1-weighting but, shorter TEs provide higher SNR [58]. At 1.5T, the optimal TE is between 40 and 60 ms, whereas between 20 and 35 at 3T [57].

The repetition time (TR)

Adequate temporal resolution is recommended to characterize the transient signal drop in the first pass of the contrast bolus. However, shorter TRs increase T1-weighting. A TR no longer than 1.5 s is recommended [59].

Flip angle(FA): Smaller flip angles decrease the unwanted T1 effect as well as reduce the baseline signal. Larger angles, although increase SNR, are undesirable in combination with short TRs (<1.5 s) because of the T1 effect [60]. The current recommendation is using a flip angle of 60-90o at 1.5T and 60-70o at 3T [54,61].

Adequate acquisition duration is necessary for sufficient characterization of the contrast bolus over time. Short acquisition time could lead to CBF and CBV errors of up to 50% especially in the context of cerebral ischemia since the bolus is commonly delayed and dispersed [62]. The whole acquisition time is usually less than 2 minutes (90-120s). It is recommended to start at least 10s before the injection of the contrast agent to

Table 1: DSC-MRI parameters table

Sequence	GE-EPI (2D multislice) rather than SE-EPI
TR/temporal resolution	1500 msec (range 1,000-1,500 msec)
TE	35-45 msec at 1.5T and 25-30 msec at 3T
Flip angle	60-70°
FOV	20x20 cm (range 20x20 to 24x24 cm)
Matrix	128x128 (range 64x64 to 256x56)
Slice thickness	5 mm (range 3-5 mm)
Number of slices	11 (range 5-20)
Interslice gap	1 mm or interleaved (range 0 to 10 mm)
Volume duration	1 TR
Scan duration	<2 min
Temporal coverage (number of volumes)	40-120 total time points
IV catheter gauge	20 gauge (range 22 to 14 gauge)
1st dose (preload)	0.025-0.1 mmol/kg, 5-10 min before the dynamin imaging
2nd dose (imaging dose)	0.1 mmol/kg, 30-50 time points after imaging begins
GBCA injection rate	5 ml/s
Saline flush	25 ml (range 20-30 ml) at same rate of GBCA

achieve a steady state in the baseline images.

Contrast Agents: Gadolinium-based contrast agents are used off-label for brain PWI as they do not have specific U.S. Food and Drug Administration (FDA) approval for this purpose [63]. This contrast agent results in shortening of T1 and T2 relaxation time. If the assumption of intact BBB is preserved, the T1 effect (positive enhancement) only remains intravascular and it is negligible [64] in comparison to T2 or T2* susceptibility effect (negative enhancement). Several studies have used gadolinium chelates at different doses and from various manufacturers [65,66]. A dose of 0.1mmol/kg body weight of gadobutrol or gadobenate dimeglumine is adequate. The contrast agent is administered intravenously at a high rate (5ml/s) to avoid bolus dispersion. A power injector is typically used [66,67]. Slow injection rate (2.5 ml/s) can create bolus dispersion and underestimation of the AIF. However, fast rate (up to 10 ml/s) does not substantially add benefit with regards to the bolus shape [68]. Moreover, injection rates higher than 5 ml/s using a small gauge access can cause significant errors [39]. To optimize the injection technique, it is recommended to inject in the right arm then flush with at least 25 mL saline at the same administered rate as the contrast agent to push the bolus toward the heart. This will assure bolus coherence, and also, reduce the risk of substantial backflow into the jugular vein [69]. **Table 1** highlights DSC-MRI parameters, optimized for GE-EPI sequence.

Post-processing and image analysis

Software packages dedicated to the analysis of DSC-imaging sequences are readily available and included in manufacturers' workstations. The continuous improvement of these computer programs offers a simpler, more rapid and robust analysis. DSC-MRI data can be analyzed by two methods:

1. Curve fitting based, also known as semi-quantitative method.
2. Deconvolution based method, also known as quantitative methods.

Both methods share the same initial steps; obtaining curves of signal change over time; estimating the baseline signal from the initial time-points before contrast injection (it is preferable to exclude the first two volumes since the steady state signal might not be reached); calculation of the concentration-time curve. To obtain quantitative parameters, further tracer kinetic modeling is needed. It is useful to examine the EPI source images for artifacts that may affect the perfusion maps. Inspection of the signal intensity-time curve is also advisable to have an idea about which whether T1 or T2* star effect is dominant.

Semi-quantitative Methods: These methods rely on the tissue concentration, which depends on the local shape of the AIF and the so-called *summary parameters* can be calculated from the concentration-time curve, see **Fig. 2**. The bolus arrival time (BAT) mainly reflects collateral circulation. The time to peak (TTP), can reflect tissue transit time, collateral circulation and cardiac ejection fraction, full width at half maximum (FWHM) depends on tissue MTT [37]. The area under the peak (AUP) is proportional to rCBV and (the peak) is the max-

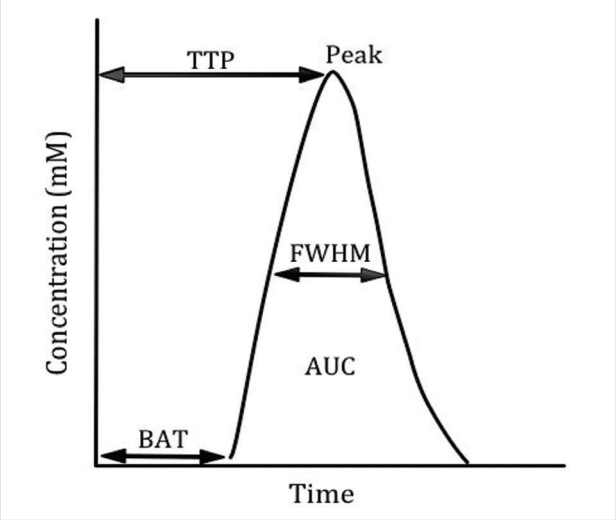

Fig. 2: Diagram of a concentration-time curve showing the summary parameters including bolus arrival time (BAT), time to peak (TTP), full-width at half-maximum concentration (FWHM), maximum peak concentration (Peak), and area under the peak (AUP)

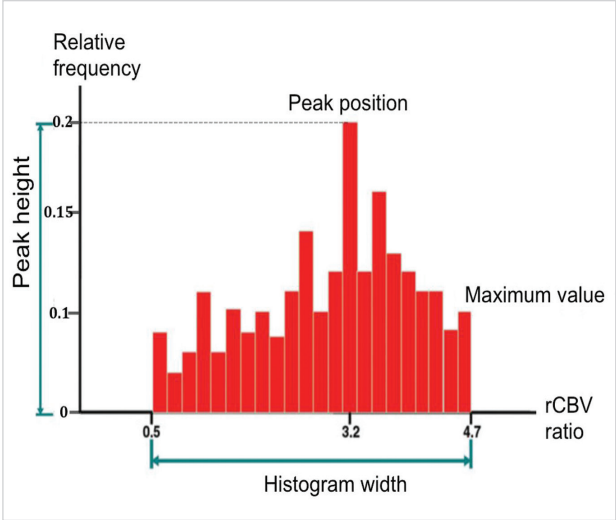

Fig. 3: Histogram parameters that are used in DSC-MRI

imum GBCA concentration, (Fig. 2). Summary parameters are easy to calculate, do not require identification of the AIF and less demanding in the SNR and temporal resolution. However, they have major disadvantages, they are non-physiological and depend on the local shape of the AIF of the specific scan and do not account for the inter-individual differences in macrovascular structure, such as arterial status, cardiac output, as well as injection technique and contrast agent leakage [70,71]. They also derived from the signal intensity, which has no physical units and can be influenced by imaging acquisition techniques. Thus, this method makes the comparison between scans obtained at different sites difficult. To improve the summary parameters, data fitting most commonly by γ-variate function and baseline subtraction methods can be applied to the concentration-time curve to correct for recirculation and contrast leakage effects [35,72]. rCBV map can be then estimated from the area under the fitted curve whereas rCBF and MTT maps could also be less accurately estimated. Therefore, when the semi-qualitative analysis is considered, it is better to use summary parameters rather than the use of physiological perfusion parameters.

Deconvolution-based method: The deconvolutional method requires the identification of AIF to produce so called the parametric (quantitative) maps. The maps then could be analyzed by "hot-spots" or histogram analysis. Although the quantitative analysis is more difficult to obtain, it is more accurate and powerful than semi-qualitative analysis because it is relatively independent of magnetic strength, scanner manufacturer, contrast injection technique, thus enables valid comparisons between scanners, subjects and in longitudinal studies. Furthermore, the derived parameters CBV, CBF and MTT are more reliable as they are physiological.

Hot-spot analysis method: Regional calculation of perfusion parameters in tumors is commonly performed by manual placement of region of interests (ROIs) around a portion, or the entire lesion [73]. Care should be taken to avoid large extra- and intratumoral vessels when placing the ROIs [74]. The most acceptable method is to draw several ROIs in the hot-spots and then to choose the ROI of the highest mean [75]. The parameters from the humoral ROIs are typically normalized to a reference ROI in the normal appearing white matter.

Histogram analysis: Histograms are generated from regions of interest drawn around the whole lesion. The area under the histogram curve is usually normalized to the value of one and classified into a predefined number of bins. Values from the ROI are plotted against the relative frequency (**Fig. 3**). The following histogram metrics can be obtained: mean value; standard deviation; peak value or position; and peak height. Histograms can give a global estimate when considering the heterogeneity of

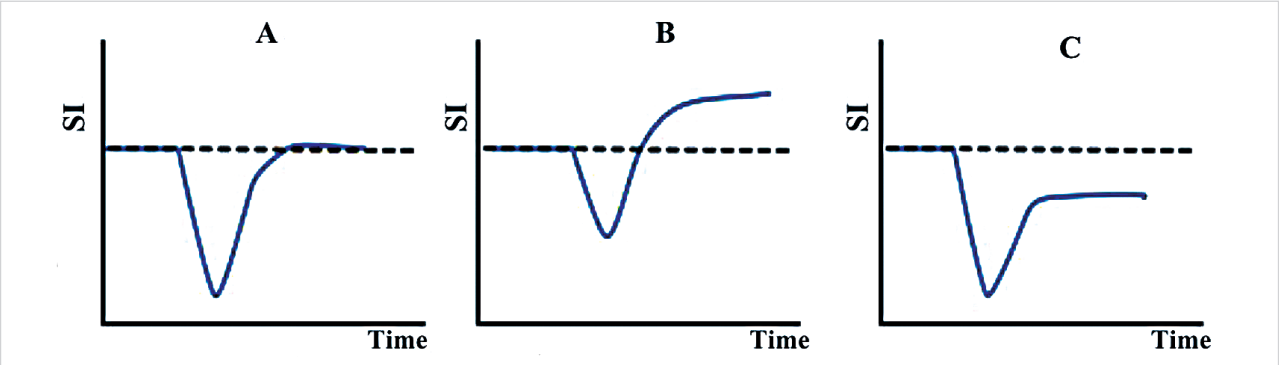

Fig. 4. *Illustration of the effect of BBB leakage on the signal-intensity time curves. A: The curve shows an intact BBB and negligible T1 effects. B: time curve with BBB leakage, the T1 effect dominates, leading to a lesser signal drop and an overshoot after the bolus passes. C: Time curve with BBB leakage, the T2* effect dominates (e.g., when a double-echo sequence is used). In B and C quantification errors will occur if the distortions to the time curves are not accounted for in the DSC-MRI model*

the tissue of interest; however, this can lead to the loss of the spatial specificity [76]. Histogram methods have been proven to have greater interobserver agreement compared with the localized hot-spot, and similar diagnostic accuracy [77,78]. Several studies have demonstrated the diagnostic value of histogram indices of perfusion parameters in brain tumor imaging [79-83].

4. Technical considerations

Arterial input function: Correct measurement of AIF, which can be challenging, is crucial for perfusion quantification to eliminate the effect of cardiac output and injection variability. Measurement of the AIF is subject to partial volume effect due to the relatively low spatial resolution of EPI acquisitions. The AIF is typically measured within or better in the immediate vicinity of a vessel; it is preferred to be perpendicular to the main magnetic field, e.g. in the middle cerebral artery. Several studies have shown that measuring AIF near but completely outside the middle cerebral artery gives a good estimate of the shape [46,84]. The most common problems are the flow-related artifacts and partial volume effects. A perfect AIF is characterized by the early time of arrival, high amplitude and small full width at half maximum [4]. An incorrect AIF leads to a systematic error in the quantification, and the wrong shape causes erroneous result after the deconvolution analysis [46]. Several automatic methods have been developed to estimate the AIF [85-87], which are less operator-dependent and more reproducible.

Arterial delay and dispersion: One AIF is used as an input function for the whole brain to quantify perfusion. In healthy vessels, dispersion of the AIF in macrovascular structures is negligible compared to the dispersion at microvascular level. Any changes in the AIF, e.g. vascular occlusion or narrowing, before the bolus reaches the tissue of interest will be propagated to the residue function and will be interpreted as microvascular dispersion leading to underestimation of the perfusion measurements [67]. The only way to differentiate between macro- and microvascularity dispersion is to measure the AIF locally, as near as possible to the tissue of interest. The main reservation of the local AIF however, is that the vessels are small, and there is, a higher chance of partial volume effect [88].

T1 effects and blood-brain barrier (BBB) leakage: The gadolinium contrast agent not only affects transverse relaxation rate but also affects the longitudinal relaxation rate, leading to T1 shortening. DSC-MRI quantification models are typically based on the assumption that contrast agent remains within the vessels. In the presence of a normal BBB, the recorded signal is largely T2*-weighted and the influence of T1 effects is negligible [60]. However, When the BBB is damaged, contrast leaks into the extracellular space, leading to a reduction in the T2* relaxation and a shortening of T1 in the extravascular tissue. These two effects can significantly reduce the signal loss caused by susceptibility effects, and lead to quantification errors in CBF and CBV [89]. The T1 effect could be minimized by using a flip angle significantly smaller than the Ernst-angle or by using dual or multiple echo sequences. Many authors have presented algorithms to correct

Table 2. Techniques for T1 leakage correction

Category	Technique	Mechanism	References
Image acquisition	long TE, small flip angle, double-echo T2*-weighted	Minimise T1 effect and increase T2 weighting.	Knopp et al. [98], Cha et al.[72], Vonken et al.[30], Uematsu et al.[99]
Contrast agent	Preload doses	The original tissue T1 is decreased after the preload, leading to minimization of the changes in T1 relaxation, which might occur during the first-pass of the contrast agent.	Donahue et al.[100], Schmainda et al.[101], Simonsen et al.[102], Boxerman et al.[96]
	Intravascular agents (eg, ferumoxytol)	Ferumoxytol has large-sized iron nanoparticlesand it acts as a blood pool agent, which does not cross the disrupted BBB in the short term.	Gahramanov et al.[103]
Post-processing	Linear fit and leakage correction modelling	MTT-*insensitive*: assumes that MTT is the same in normal and abnormal tissues. The algorithm is based on the linear fit of the obtained curve to constant functions derived from non-enhancing brain tissues. However, it may give errors in tumors with marked leakage as MTT is usually prolonged.	Schmainda et al.[101], Boxerman et al.[44]
		MTT-*sensitive*: accounts for differences in tissue MTT by estimating contrast leakage from the tissue residue function.	Quarles et al.[97], Bjornerud et al.[93]
	γ-variate fit	A non-linear gamma-variate function is fitted to the signal intensity-time. It approximates the curve shape that would have been obtained without leakage or recirculation.	Rosen et al.[35], Benner et al.[104] Lee et al.[105], Law et al.[106]
	Limited integration	Use only the integration from the beginning of the bolus to the peak curve before T1 effects become more evident.	Wong et al.[107]
	Baseline subtraction	The baseline values are calculated from a line between the beginning and end of the first pass then subtracted from the measurements obtained during the passage of the bolus through the tissue.	Cha et al.[108], Wetzel et al.[75]

for the contrast agent leakage and thus minimization of the T1 effect [44,90,91]. Nevertheless, these algorithms require tracer kinetic modeling and an appropriate pulse sequence. Another approach to minimize T1 leakage effect is to give a preload consisting of a small amount of the contrast agent [92]. This preload dose will reduce the concentration gradients between the vessels and the tissue that drive the leakage and thus lower the T1 value of the extravascular compartment. Specifically, it is assumed that the T1 relaxation largely saturated, and no further shortening of T1 will occur.

When the T1 effect is removed, it is quite often that the measured perfusion may be over-estimated due to the so- called T2* effect or T2* leakage (**Fig. 4**). Several post-processing methods have been proposed to correct for T1- and T2*-dominated leakage effects [93,94]. Paulson and Schmainda suggested in their study, performed on 22 high-grade gliomas, that a dual-echo sequence or

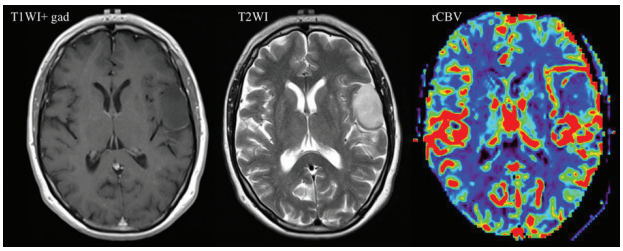

Fig. 5: *Non-enhanced mass in the left inferior frontal gyrus, with decreased blood volume. Pathology demonstrated astrocytoma WHO grade II*

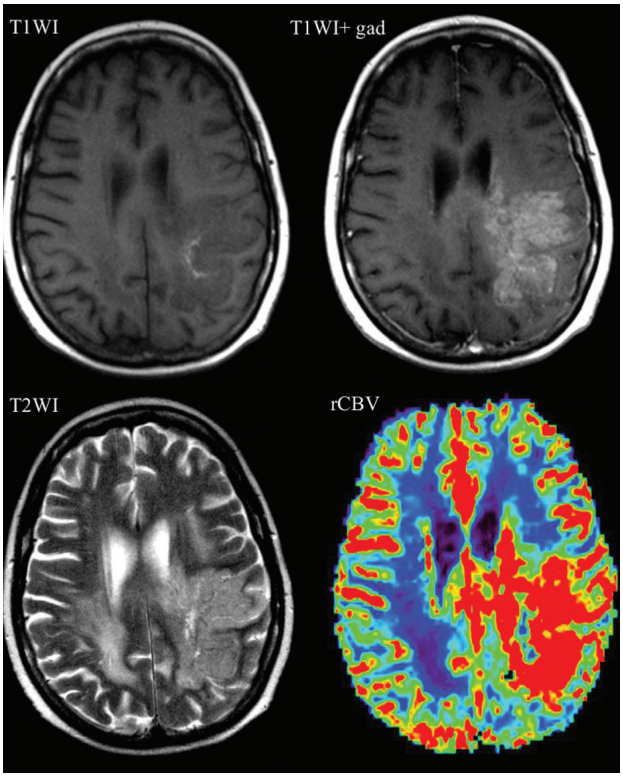

Fig. 6: *Right fronto-parietal GBM. Pre and post contrast T1WI showed subacute hemorrhage and contrast enhancement respectively. The mass is hyperintense in T2WI with late subacute hemorrhagic changes. rCBV map demonstrates high perfusion*

a preload of contrast, combined with a post-processing correction of T2*/T2 effects, may provide the most accurate approach for measuring CBV in tumors [95]. T1 leakage correction can be classified into three schemes explained in **Table 2** [96]. A note should be made here that despite the substantial errors in uncorrected CBV caused by BBB leakage, errors from uncorrected CBF are much less severe [97].

Limitations: DSC-MRI is a susceptibility-weighted technique that is sensitive to any strong magnetic field inhomogeneity, which can be caused by calcium, blood products, melanin, metal depositions or at the brain-bone-air interface. Macroscopic susceptibility may be reduced by increasing the spatial resolution, but this would be a trade off on the expense of the coverage area and signal-to-noise ratio. Another disadvantage of the DSC-MRI technique is the requirement for injection of gadolinium, which can be limited by concerns related to toxicity [109,110]. There are also limitations in the CBV calculation in the context of damaged BBB unless appropriate measures are taken. Finally, a major limitation of DSC-MRI is the lack of technical standardization in acquisition and post-processing methods. Perfusion measurements tend to be relative, because their quantification is dependent on the methods, such as the AIF selection, deconvolution methods, and the interplay of T1 and T2* effects adds more complexity to the measurements [54].

5. Clinical Applications

DSC-MRI has shown great potential in brain tumor imaging. The derived parameters are relative CBV, CBF and MTT (rCBV, rCBF and MTT). rCBV, in particular, is the most reliable parameter for characterization of brain tumors, MTT is the least [29].

Primary diagnosis and grading

Accurate glioma grading is crucial for patient management and outcome. The current standard method of grading is histological assessment, but this has limitations. Firstly, it is restricted due to the invasive nature of the procedure. Secondly, gliomas are inherently heterogeneous and sampling only one region may lead to errors and underestimation of glioma grade in 30% of cases [111]. Thirdly, besides the spatial heterogeneity of gliomas, angiogenesis demonstrates a considerable temporal heterogeneity, and therefore tumor angiogenesis, and grade may significantly change with time, rendering sampling at one-time point potentially ineffective. Finally, for reliable assessment of the humoral changes in glioma, it is inconvenient to repeat an invasive procedure frequently to assess a process that differs in time and space, especially in the setting of anti-angiogenic therapies. These limitations have encouraged the development of imaging-based grading methods, and the assessment of angiogenesis that can be measured and quantified by perfusion MRI plays a pivotal role in this [112,113].

Table 3: Listed values of rCBV and rCBF for high- and low-grade gliomas, HGG and LGG respectively. N, the number of cases; A, GBM only; B, anaplastic astrocytoma only; C, oligoastrocytoma; D, oligodendroglioma; E, nonenhancing astrocytomas

Authors	N	HGG range (mean) or Mean ± SD		LGG range (mean) or Mean ± SD	
		rCBV	rCBF	rCBV	rCBF
Aronen et al.[114]	19	0.8-5.4 (3.6)		1.1-1.2 (1.1)	
Sugahara et al.[120]	30	4.0-16.2 (7.3)[A]		0.6-2.01 (1.3)	
		0.98-7.9 (4.6)[B]			
Knop et al. [98]	29	1.7-13.7 (5.07)		0.92-2.19 (1.44)	
Shin et al.[121]	17	0.9-7.9 (4.9)	1.3–11.2 (4.8)	0.72-5.1 (2)	0.82-3.4 (1.8)
Law et al.[12]	160	0.96-19.8 (5.18)		0.77-9.8 (2.1)	
Hakyemez el al.[122]	33	2.4-18.6 (6.5)	1.4-8.7 (3.3)	0.97-2.88 (1.7)	0.8-2.2 (1.16)
Bai et al.[123]	33	5.71 ± 1.63		1.67 ± 0.43	
Law et al.[106]	73	6.05 ± 2.22A		1.75 ± 0.85	
		3.79 ± 1.48B			
Cho et al.[124]	29	3.02-16.7 (9.3)		1.30-5.07 (3.64)	
Lee et al.[105]	22	4.90 ± 1.01A		1.75 ± 1.51	
		3.97 ± 0.56B			
Saito et al.[125]	24			2.01 ± 0.68	
				4.60 ± 1.05C	
				6.17 ± 0.867D	
Cha et al.[115]	25			0.48-1.3(0.2)	
				1.3-9.2 (3.7)D	
Arvinda[126]	51	2.8-12.9 (3.3)		0.29-3.14 (1.2)	
Castanzo[126]	36	4.3 ± 1.2		2.0 ± 1.5	
Morita et al.[118]	17	1.11 ± 0.13E		0.66 ± 0.17	

Gliomas can have marked histologic heterogeneity. Therefore, the overlap of rCBV measurements between different glioma grades is an important issue to recognize. The rCBV maps of gliomas should not be interpreted without conventional MR images, as these can provide other valuable information [72]. The maximum rCBV value correlates with the tumor's mitotic activity and vascularity, as initially observed by Aronen et al. [114]. Low-grade astrocytomas tend to demonstrate little to no rCBV elevation compared to the contralateral normal appearing brain [98] (**Fig.5**). Among high-grade gliomas, anaplastic astrocytomas tend to demonstrate lower relative CBV measurements in comparison to GBM [115] (**Fig.6**). Grading of non-enhancing astrocytomas can be challenging with conventional contrast-enhanced MRI as 20% of low-grade gliomas enhance, and approximately one-third of non-enhancing gliomas are malignant [116,117]. Measurements of rCBV increase the accuracy of grading of non-enhancing astrocytomas [118].

Table 3 lists the results of previous PWI for glial tumors. It is observed from the table that low and high-grade tumors have entirely different ranges of the mean rCBV.

Table 4: A list of rCBV and rCBF thresholds for distinguishing low- from high-grade gliomas. N, number of cases A, non-enhancing astrocytoma; B, GBM *vs* CNS lymphoma; C, GBM *vs* metastasis; D, GBM *vs* grade 3 glioma; E, GBM *vs* grade 2 glioma; F, Grade 3 *vs* Grade 2 glioma

	N			Cut-off value	Sensitivity	Specificity	PPV	NPV
Shin et al.[121]	17	rCBV		2.93	90.9	83.3		
		rCBF		3.57	72.7	100		
Law et al.[12]	160	rCBV		1.75	95	57.5	87	79.3
Lev et al.[128]	32	rCBV		1.5	100	69		
Hakyemez et al.[122]	33	rCBV		2	100	90.9		
		rCBF		1.3				
Arvind et al.[126]	51	rCBV		2.91	94.7	93.75	90	96.3
Young et al.[83]	92	rCBV		2.15	95.1	80.65		
Morita et al.[118]	17	rCBV	A	0.94	90.9	100		
Antonio at al.[13]	21	rCBV	A	1.2	80	100		
Weber et al.[129]	97	rCBF	B	1.2	97	80	94	89
			C	0.5	100	71	94	100
			D	1.4	97	50	84	86
			E	1.6	94	78	94	78
			F	1	92	33	65	75

High-grade gliomas range between 3.64 and 9.33, while all low-grade gliomas, excluding oligodendroglial tumors, vary from 1.11 to 3.64. Many rCBV cut-off ratios have been proposed in the literature to differentiate between high and low-grade gliomas, with 1.75 rCBV ratios, probably, the most accepted one [12]. It has 95% sensitivity, 57.5% specificity, 87% positive predictive value (PPV), and 79.3% negative predictive value (NPV). This cutoff point can also be used to predict patient outcome independent from histopathology [119]. **Table 4** lists some of the rCBV and rCBF threshold from previous studies.

The increase of rCBV measurements over time can also detect malignant transformation of low-grade gliomas, which may occur up to 12 months before contrast enhancement becomes apparent on an enhanced T1 weighted imaging [130]. Finally, grading of gliomas should be ideally obtained by histologic examination of the most malignant region in the specimen. A biopsy is usually guided by enhanced T1 weighted MRI or CT scans [131]. These demonstrate the areas of disrupted BBB, which are not necessarily the most biologically aggressive regions. CBV maps, in contrast, can demonstrate regions of high vascular densities which can be targeted for stereotactic biopsy and thus reduce the sampling error [13].

Besides tumor grade prediction and biopsy guiding, CBV measurements can be helpful in the differential diagnosis of brain tumors. For instance, it is frequently difficult to differentiate between lymphoma and high-grade glioma on conventional imaging; however, in DSC-MRI lymphomas have usually significantly lower rCBV values than malignant glial tumors [132]. Peritumoral infiltration, which is a distinct feature of gliomas can be lead to increased peritumoral rCBV values [133]. This may differentiate glioma from several conditions such as solitary metastases, which may have elevated rCBV values in the tumor tissue resembling high-grade gliomas. However, due to perilesional edema and lack of peritumoral infiltration, solitary metastases demonstrate low rCBV values in the surrounding edematous white matter [134]. Similarly, a tuberculoma can present with high lesional rCBV value and low peri-lesional value for the same reason [135]. Weber et al. [129] could differentiate between GBM and CNS lymphoma as GBM has a higher blood flow; specifically, they applied a threshold value of 1.2 of DSC-derived rCBF, which provided 97% sensitivity; 80% specificity; 94% PPV, and 89% NPV. They also could differentiate between GBM and metastasis by rCBF measurement in peritumoral regions, which were found to be

significantly higher in GBM compared with metastases; here, a threshold value of 0.5 demonstrated 100% sensitivity; 71% specificity; 94% PPV; and 100% NPV [129].

Increased vascularization does not necessarily indicate malignancy [72]. Grade 2 oligodendroglioma is an example of a low-grade tumor with high rCBV [115,136]. The increased rCBV measurements in oligodendroglioma are due to the increase in the expression of morphologically delicate microvasculature [98]. Saito et al. [125] conducted a study on grade 2 and 3 astrocytic and oligodendroglial tumors; they have shown that rCBV values in oligodendroglial tumors are significantly higher than those in astrocytic tumors of a similar histological grade. The highest rCBV was found in oligodendroglioma followed by oligoastrocytoma and astrocytoma (**Fig. 7 & 8**). They also optimized a cut-off value of 3.0 that allowed differentiation between the oligodendroglial and astrocytic groups at 100% sensitivity and 87.5% specificity [125]. Whitemore et al. [137] have indicated that rCBV measurements may even predict oligodendroglial tumor subtype and grade. They found that grade 2 oligodendroglial tumor with the loss of heterozygosity (LOH) of chromosomes 1p or 1p and 19q had significantly higher rCBV than tumors without LOH. LOH was not associated with significant rCBV differences in grade 3 oligodendroglial tumors. Another low-grade tumor that demonstrates elevated rCBV is the nidus of a hemangioblastoma, a feature that helps it to differentiate it from pilocytic astrocytomas, which can appear similar to conventional images [124]. Tumefactive demyelinating lesions may cause a diagnostic dilemma by mimicking high-grade glial neoplasms on conventional MR sequences. Differentiating between these two conditions is important since demyelinating lesions require no aggressive intervention such as surgery or even biopsy [138]. CBV measurements show the hypo-perfused nature of demyelinating lesions in contrast to high-grade neoplasms [108].

Management Planning and Monitoring: Areas of higher rCBV within a tumor may respond better to chemoradiation compared to areas with low rCBV because poor circulation diminishes exposure to the chemotherapeutic agent [139]. Bisdas et al. [140] had demonstrated that rCBV values in gliomas -excluding tumors with oligodendroglial components- are more accurate predictors of recurrence and 1-year survival than histopathologic grading [140]. Furthermore, rCBV can help to identify low-grade gliomas that may progress rapidly to malignant transformation [141]. A study conducted by Law et al. [142] concluded that patients with high- and low-grade gliomas with an rCBV above 1.75 had a significantly more rapid time to progression than patients who had gliomas with an rCBV less than 1.75 [142]. rCBV measurements not only correlated well with time to progression but also with overall survival [143]. Those observations have an impact on management plan; low-grade gliomas with high rCBV values should be treated more aggressively while gliomas with low rCBV values could be treated more conservatively and might be monitored over time [144]. Thus, rCBV can act as a biomarker to examine the lesions' malignant potential and stratify them for treatment decisions and prognosis [119]. It has also been suggested that pre-treatment rCBV measurements may also be used as a prognostic biomarker for oligodendrogliomas [145]. One study validated an rCBV threshold value of 2.2 for three-year survival prognosis in patients with oligodendrogliomas demonstrating 89% and 59% sensitivity and specificity, respectively [146].

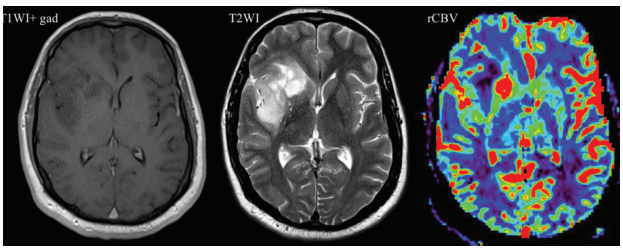

Fig. 7: *Non-enhanced mass in the right insula extending to the basal ganglia, rCBV map. Showed incresed blood volume in the striatocapsular region. Histopathological diagnosis was oligodendroglioma who grade II*

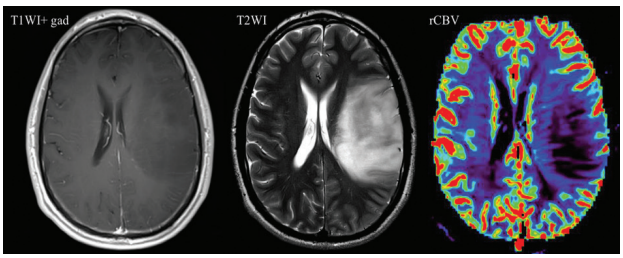

Fig. 8: *Non-enhanced mass in the left frontal lobe, with decreased blood volume. Pathology showed oligoastrocytoma WHO grade II*

Effect of glucocorticoids on DSC-MRI measurements: Glucocorticoids are often used in patients with cerebral mass to treat symptoms associated with raised intracranial pressure. Dramatic improvement in symp-

toms has been observed up to few minutes after administration, which is believed to reflect the decrease in intracranial pressure [147,148]. The mechanism is not entirely understood. It has been hypothesized that the reduction in edema and intracranial pressure are caused by tightening of the blood-tumor barrier, changes in the water homeostasis in the brain, or as a result of a decrease in rCBV [149,150]. Decreased tumoral contrast enhancement is a known feature in conventional imaging after steroid therapy [151]. Quantitative permeability parameters are also decreased [151] except for meningioma. Perfusion measurements before and after steroid treatment are variable in studies in the literature from unchanged to significant increased or decreased perfusion. Among the reported results, a trend for decreased rCBV/ MTT, whereas rCBF is increased or unchanged, has been observed [149,150,152-155]. Improved rCBF in the peritumoral edematous brain has also been demonstrated and explained by the reduced peritumoral edema [150].

Tumor response versus treatment-related conditions: The current widely used treatment strategy for high-grade tumors is maximal safe tumor resection followed by radiotherapy and chemotherapy (usually temozolomide) [156]. Up to 30% of treated patients show increased contrast enhancement in conventional imaging within the first few months, which subsequently diminishes without any additional therapy. This condition is coined as pseudoprogression opposed to the actual tumor growth [157]. Pseudoprogression results from a transient increase in the permeability of the tumor vessels due to radiation, a phenomenon that may be enhanced by temozolomide, and it is often associated with extensive edema [158,159]. A similar effect could be seen after reducing the steroid administration dose [160]. rCBV measurements can be helpful as real tumor progression has significant higher rCBV values than pseudoprogression [161-164].

Conventional chemotherapy targets mitotic activity of the tumor; however, it has poor performance in treating recurrent gliomas [165,166]. Several antiangiogenic drugs have been used in clinical trials as a new regimen for recurrent glioma. These drugs suppress angiogenesis by inhibiting VEGF (vascular endothelial growth factor) [15,167]. Both DSC and DCE can be used to assess the effectiveness of therapy. Furthermore, serial rCBV measurements correlate well with patients' clinical status [139,168-173]. Nonetheless, early after bevacizumab treatment, a commonly used antiangiogenic agent, decreased contrast enhancement is found due to normalization of the leaky dilated blood vessels in the tumor [174]. Normalization of blood vessels includes tightening of the blood-tumor barrier and a decrease in vessel diameter leading to improving CBF but decreasing CBV [175]. Decreased CBV values and vessels diameters were observed as early as one day after treatment and persisted for 28 days [176]. These apparent early responses to antiangiogenic therapy are mainly related to vascular normalization rather than treatment response. For that reason, the condition is called pseudoresponse and can be mistaken with true treatment response [174]. Vascular normalization was found to be reversible in patients undergoing a "drug holiday" [176]. It is unclear how perfusion can differentiate pseudoresponse from the true response at this stage.

Furthermore, differentiation between radiation necrosis and the recurrent tumor can be difficult with conventional imaging. Both disease processes can cause diffuse white matter abnormalities either due to tumor infiltration or the demyelination process of radiation necrosis. Both also involve a degree of BBB disruption resulting in contrast enhancement on conventional imaging [177]. Differentiating between radiation necrosis and the recurrent tumor is important. As recurrent tumors can be managed by surgery, adjuvant chemotherapy or targeted high dose radiation therapy, radiation necrosis may be treated conservatively with steroids [72]. rCBV measurements tend to be elevated in tumor recurrence due to increased vascularity, whereas, in radiation necrosis, they are usually lower than normal [177-179].

6. The present and future of DSC-MRI

Over the last decade, DSC-MRI underwent significant developments regarding acquisition techniques and post-processing methods, encouraged by emerging new treatment strategies of brain tumors and the urge to find reliable non-invasive methods for longitudinal assessment of subtle regression, progression or therapy-induced tissue injury. Perfusion DSC-MRI indices are widely used in clinical trials as biomarkers to assess treatment responses [79,146,177,180-186] and despite the proven benefits the technique is not widely used in clinical practice. The lack of agreed standards for data acquisition and post-processing techniques is a major challenge for

inter-site comparison and meta-analysis studies. Standardization of the technique is essential for clinically reproducible measurements across multiple institutions [187-190]. Additionally, for DSC-MRI to be a relevant imaging endpoint for neuro-oncology clinical trials it needs validation, by such as test-retest methods to ensure that the radiographic response reflects therapeutic antitumor effect.

Methodology-wise, DSC-MRI post-processing techniques are largely mature and will continue to benefit from hardware and software developments in the future. However, much work is required to address the limitations above and to establish consensus-based recommendations for imaging protocols, data modeling, analysis, and interpretation. Considering the diversity of the applications of DSC-MRI in neuroimaging, such recommendations would not only ease the comparison across sites but also facilitate the clinical dissemination. Moreover, DSC- MRI has to clearly prove that its impact on the patient management strategy is crucial to the patient survival and the therapy response, whereas health economics issues also have to be encountered in the broad application of the technique in clinical routine.

7. Conclusion

DSC-MRI is a robust imaging technique for estimating brain perfusion and has marked advantages in the context of brain neoplasms where contrast leakage and spatial heterogeneity are commonly expected. This article introduced the reader to the basic principles of DSC-MRI and reviewed the clinical value of DSC-MRI in primary and secondary brain tumors in various settings. It is important to consider this useful imaging method as complementary; a multiparametric approach is expected to provide a better evaluation of brain tumors and should be pursued in the clinical practice. **R**

Conflict of interest:
The authors declared no conflicts of interest.

References

1. Guyton AC, Hall JE. Textbook of medical physiology. Eleventh edition; *W B Saunders Company* 2006: 673-768.
2. Raichle ME, Mintun MA. Brain work and brain imaging. *Annual Review of Neuroscience* 2006; 29(1): 449-476.
3. Lantz BM, Foerster JM, Link DP, et al. Regional distribution of cardiac output: Normal values in man determined by video dilution technique. *American Journal of Roentgenology* 1981; 137(5): 903-907.
4. Barker PB, Golay X, Zaharchuk G. Clinical Perfusion MRI. *Cambridge University Press* 2013; 505.
5. Cuenod CA, Balvay D. Perfusion and vascular permeability: Basic concepts and measurement in DCE-CT and DCE-MRI. *Diagnostic and Interventional Imaging Elsevier Masson SAS* 2013; 94(12): 1187-1204.
6. Ryu CW, Lee DH, Kim HS, et al. Acquisition of MR perfusion images and contrast-enhanced MR angiography in acute ischaemic stroke patients: Which procedure should be done first? *British Journal of Radiology* 2006; 79(948): 962-967.
7. Lin K, Kazmi KS, Law M, et al. Measuring elevated microvascular permeability and predicting hemorrhagic transformation in acute ischemic stroke using first-pass dynamic perfusion CT imaging. *AJNR Am J Neuroradiol* 2007; 28(7): 1292-1298.
8. Siemund R, Cronqvist M, Andsberg G, et al. Cerebral perfusion imaging in hemodynamic stroke: Be aware of the pattern. *Interv Neuroradiol. Centauro Srl* 2009; 15(4): 385-394.
9. Zaharchuk G. Arterial spin labeling for acute stroke: Practical considerations. Transl Stroke Res. *Springer-Verlag* 2012; 3(2): 228-235.
10. Wang DJJ, Alger JR, Qiao JX, et al. Multi-delay multi-parametric arterial spin-labeled perfusion MRI in acute ischemic stroke - Comparison with dynamic susceptibility contrast enhanced perfusion imaging. *NeuroImage: Clinical* 2013; 3: 1-7.
11. Hartkamp NS, Petersen ET, De Vis JB, et al. Mapping of cerebral perfusion territories using territorial arterial spin labeling: techniques and clinical application. *NMR Biomed* 2013; 26(8): 901-912.

12. Law M, Yang S, Wang H, et al. Glioma grading: Sensitivity, specificity, and predictive values of perfusion MR imaging and proton MR spectroscopic imaging compared with conventional MR imaging. *AJNR Am J Neuroradiol. American Society of Neuroradiology* 2003; 24(10): 1989-1998.
13. Maia ACM, Malheiros SMF, da Rocha AJ, et al. Stereotactic biopsy guidance in adults with supratentorial nonenhancing gliomas: Role of perfusion-weighted magnetic resonance imaging. *J Neurosurg.* 2004; 101: 970-976.
14. Lev MH, Ozsunar Y, Henson JW, et al. Glial tumor grading and outcome prediction using dynamic spin-echo MR susceptibility mapping compared with conventional contrast-enhanced MR: Confounding effect of elevated rCBV of oligodendrogliomas. *AJNR Am J Neuroradiol* 2004; 25: 214-221.
15. Lupo JM, Cha S, Chang SM, et al. Dynamic susceptibility-weighted perfusion imaging of high-grade gliomas: Characterization of spatial heterogeneity. *AJNR Am J Neuroradiol* 2005; 26: 1446-1454.
16. Chung WJ, Kim HS, Kim N, et al. Recurrent glioblastoma: Optimum area under the curve method derived from dynamic contrast-enhanced T1-weighted perfusion MR imaging. *Radiology* 2013;269: 561-568.
17. Yamamoto T, Kinoshita K, Kosaka N, et al. Monitoring of extra-axial brain tumor response to radiotherapy using pseudo-continuous arterial spin labeling images: Preliminary results. *Magnetic Resonance Imaging* 2013; 31: 1271-1277.
18. Arevalo-Perez J, Kebede AA, Peck KK, et al. Dynamic Contrast-Enhanced MRI in Low-Grade *vs* Anaplastic Oligodendrogliomas. *Journal of Neuroimaging* 2016; 26: 366-371.
19. Smievoll AI, Engelsen B, Karlsen BE, et al. Perfusion-weighted (PW) and flair-weighted magnetic resonance imaging (MRI) for local diagnosis in epilepsy. *NeuroImage* 2000; 11: S162.
20. Oner AY, Eryurt B, Ucar M, et al. pASL *vs* DSC perfusion MRI in lateralizing temporal lobe epilepsy. *Acta Radiol* 2015; 56: 477-481.
21. Sierra-Marcos A, Carreño M, Setoain X, et al. Accuracy of arterial spin labeling magnetic resonance imaging (MRI) perfusion in detecting the epileptogenic zone in patients with drug-resistant neocortical epilepsy: Comparison with electrophysiological data, structural MRI, SISCOM and FDG-PET. *Eur J Neurol* 2016; 23: 160-167.
22. Wakisaka K, Morioka T, Shimogawa T, et al. Epileptic Ictal Hyperperfusion on Arterial Spin Labeling Perfusion and Diffusion-Weighted Magnetic Resonance Images in Posterior Reversible Encephalopathy Syndrome. *J Stroke Cerebrovasc Dis* 2016; 25: 228-237.
23. Bozzao A, Floris R, Baviera ME, et al. Diffusion and perfusion MR imaging in cases of Alzheimer's disease: Correlations with cortical atrophy and lesion load. *AJNR Am J Neuroradiol. American Society of Neuroradiology* 2001; 22: 1030-1036.
24. Kamagata K, Motoi Y, Hori M, et al. Posterior hypoperfusion in Parkinson's disease with and without dementia measured with arterial spin labeling MRI. *J Magn Reson Imaging* 2011; 33: 803-807.
25. Gupta RK, Awasthi R, Garg RK, et al. T1-weighted dynamic contrast-enhanced MR evaluation of different stages of neurocysticercosis and its relationship with serum MMP-9 expression. *AJNR Am J Neuroradiol. American Society of Neuroradiology.* 2013; 34: 997-1003.
26. Lacalle-Aurioles M, Alemán-Gómez Y, Guzmán-De-Villoria JA, et al. Is the cerebellum the optimal reference region for intensity normalization of perfusion MR studies in early Alzheimer's disease? *Lakshmana MK* 2013; 8: e81548.
27. Mak HKF, Chan Q, Zhang Z, et al. Quantitative assessment of cerebral hemodynamic parameters by QUASAR arterial spin labeling in Alzheimer's disease and cognitively normal Elderly adults at 3-tesla. *J Alzheimers Dis* 2013; 31: 33-44.
28. Cramer SP, Larsson HBW. Accurate determination of blood-brain barrier permeability using dynamic contrast-enhanced T1-weighted MRI: A simulation and in vivo study on healthy subjects and multiple sclerosis patients. *J Cereb Blood Flow Metab* 2014; 34: 1655-1665.
29. Milchenko MV, Rajderkar D, LaMontagne P, et al. Comparison of Perfusion- and Diffusion-weighted Imaging Parameters in Brain Tumor Studies Processed Using Different Software Platforms. *Academic Radiology* 2014; 21: 1294-1303.
30. Hahn OM, Yang C, Medved M, et al. Dynamic contrast-enhanced magnetic resonance imaging pharmacodynamic biomarker study of sorafenib in metastatic renal carcinoma. *J Clin Oncol.* 2008; 26: 4572-4578.

31. Jain R, Scarpace LM, Ellika S, et al. Imaging response criteria for recurrent gliomas treated with bevacizumab: Role of diffusion weighted imaging as an imaging biomarker. *J Neurooncol* 2010;96: 423-431.
32. Chung C, Jalali S, Foltz W, et al. Imaging Biomarker Dynamics in an Intracranial Murine Glioma. *Study of Radiation and Antiangiogenic Therapy.* 2013; 85: 805-812.
33. Hales PW, Phipps KP, Kaur R, et al. A Two-Stage Model for *in Vivo* Assessment of Brain Tumor Perfusion and Abnormal Vascular Structure Using Arterial Spin Labeling. *Platten M* 2013; 8: e75717.
34. Villringer A, Rosen BR, Belliveau JW, et al. Dynamic imaging with lanthanide chelates in normal brain: Contrast due to magnetic susceptibility effects. *Magn Reson Med* 1988;6: 164-174.
35. Rosen BR, Belliveau JW, Vevea JM, et al. Perfusion imaging with NMR contrast agents. *Magn Reson Med.* 1990; 14: 249-265.
36. Calamante F, Thomas DL, Pell GS, et al. Measuring Cerebral Blood Flow Using Magnetic Resonance Imaging Techniques. Journal of Cerebral Blood Flow & *Metabolism* 1999; 19: 701-735
37. Ostergaard L. Principles of cerebral perfusion imaging by bolus tracking. *J Magn Reson Imaging* 2005; 22: 710-717.
38. Calamante F. Perfusion MRI using dynamic-susceptibility contrast MRI: Quantification issues in patient studies. *Top Magn Reson Imaging* 2010;21: 75-85.
39. Shiroishi MS, Castellazzi G, Boxerman JL, et al. Principles of T2*-weighted dynamic susceptibility contrast MRI technique in brain tumor imaging. *J Magn Reson Imaging* 2014; 41: 296-313.
40. Xu B, Spincemaille P, Liu T, et al. Quantification of cerebral perfusion using dynamic quantitative susceptibility mapping. *Magn Reson Med.* 2015; 73: 1540-1548.
41. Ostergaard L, Weisskoff RM, Chesler DA, et al. High resolution measurement of cerebral blood flow using intravascular tracer bolus passages. Part I: Mathematical approach and statistical analysis. *Magn Reson Med* 1996; 36: 715-725.
42. Lassen NA, Perl W. Tracer kinetic methods in medical physiology. *Raven Press New York* 1979; ix: 189.
43. Sourbron S. A tracer-kinetic field theory for medical imaging. *IEEE Trans Med Imaging* 2014;33: 935-946.
44. Boxerman JL, Schmainda KM, Weisskoff RM. Relative cerebral blood volume maps corrected for contrast agent extravasation significantly correlate with glioma tumor grade, whereas uncorrected maps do not. *AJNR Am J Neuroradiol* 2006; 27: 859-867.
45. Calamante F. Arterial input function in perfusion MRI: A comprehensive review. *Prog Nucl Magn Reson Spectrosc* 2013; 74: 1-32.
46. Bleeker EJ, van Buchem MA, van Osch MJ. Optimal location for arterial input function measurements near the middle cerebral artery in first-pass perfusion MRI. Journal of Cerebral Blood Flow & *Metabolism* 2009; 29: 840-852.
47. Ostergaard L, Sorensen AG, Kwong KK, et al. High resolution measurement of cerebral blood flow using intravascular tracer bolus passages. Part II: Experimental comparison and preliminary results. *Magn Reson Med.* 1996; 36: 726-736.
48. Tofts P. Quantitative MRI of the Brain. First edition. John Wiley & Sons. 2003.PP, 366-412.
49. Duyn JH, van Gelderen P, Barker P, et al. 3D bolus tracking with frequency-shifted BURST MRI. *J Comput Assist Tomogr* 1994;18: 680-687.
50. Rempp KA, Brix G, Wenz F, et al. Quantification of regional cerebral blood flow and volume with dynamic susceptibility contrast-enhanced MR imaging. *Radiology* 1994;193: 637-641.
51. Wirestam R, Andersson L, Ostergaard L, et al. Assessment of regional cerebral blood flow by dynamic susceptibility contrast MRI using different deconvolution techniques. *Magn Reson Med* 2000; 43: 691-700.
52. Perman WH, Gado MH, Larson KB, et al. Simultaneous MR Acquisition of Arterial and Brain Signal-Time Curves 1992. *Perman* 2005; 28: 74-83.
53. Pedersen M, Klarh fer M, Christensen SR, et al. Quantitative cerebral perfusion using the PRESTO acquisition scheme. *J Magn Reson Imaging.* 2004; 20: 930-940.
54. Willats L, Calamante F. The 39 steps: Evading error and deciphering the secrets for accurate dynamic susceptibility contrast MRI. Lu H, editor. *NMR Biomed* 2013; 26: 913-931.
55. Heiland S, Kreibich W, Reith W, et al. Comparison of echo-planar sequences for perfusion-weighted MRI: Which is best? 1998; 40: 216-221.
56. Boxerman JL, Hamberg LM, Rosen BR, et al. Mr Contrast Due to Intravascular Magnetic-Susceptibility Perturbations. *Magn Reson Med* 1995; 34: 555-566.
57. Thilmann O, Larsson EM, Björkman-Burtscher IM,

et al. Effects of echo time variation on perfusion assessment using dynamic susceptibility contrast MR imaging at 3 tesla. *Magnetic Resonance Imaging* 2004; 22: 929-935.

58. Smith MR, Lu H, Frayne R. Signal-to-noise ratio effects in quantitative cerebral perfusion using dynamic susceptibility contrast agents. *Magn Reson Med*. 2003; 49: 122-128.
59. Knutsson L, Ståhlberg F, Wirestam R. Aspects on the accuracy of cerebral perfusion parameters obtained by dynamic susceptibility contrast MRI: A simulation study. *Magnetic Resonance Imaging* 2004; 22: 789-798.
60. Calamante F, Vonken E-JPA, van Osch MJP. Contrast agent concentration measurements affecting quantification of bolus-tracking perfusion MRI. *Magn Reson Med* 2007; 58: 544-553.
61. Welker K, Boxerman J, Kalnin A, et al. ASFNR recommendations for clinical performance of MR dynamic susceptibility contrast perfusion imaging of the brain. *AJNR Am J Neuroradiol* 2015; E41-E51.
62. Calamante F. Bolus dispersion issues related to the quantification of perfusion MRI data. *J Magn Reson Imaging* 2005; 22: 718-722.
63. Essig M, Nguyen TB, Shiroishi MS, et al. Perfusion MRI: The Five Most Frequently Asked Clinical Questions. *American Journal of Roentgenology* 2013; 201: W495-W510.
64. Roberts TPL, Mikulis D. Neuro MR: Principles. *J Magn Reson Imaging* 2007; 26: 823-837.
65. Tombach B, Benner T, Reimer P, et al. Do Highly Concentrated Gadolinium Chelates Improve MR Brain Perfusion Imaging? Intraindividually Controlled Randomized Crossover Concentration Comparison Study of 0.5 *vs* 1.0 mol/L *Gadobutrol*. 2003; 226: 880-888.
66. Thilmann O, Larsson E-M, Björkman-Burtscher IM, et al. Comparison of contrast agents with high molarity and with weak protein binding in cerebral perfusion imaging at 3 T. *J Magn Reson Imaging*. 2005; 22: 597-604.
67. Knutsson L, Ståhlberg F, Wirestam R. Absolute quantification of perfusion using dynamic susceptibility contrast MRI: pitfalls and possibilities. *Magn Reson Mater Phy*. 2009;23: 1-21
68. van Osch MJP, Vonken E-JPA, Viergever MA, et al. Model of the human vasculature for studying the influence of contrast injection speed on cerebral perfusion MRI. *Magn Reson Med* 2003; 50: 614-622.
69. Jackson A. Analysis of dynamic contrast enhanced MRI. *British Journal of Radiology* 2004; 77(2): S154-S166.
70. Weisskoff RM, Chesler D, Boxerman JL, et al. Pitfalls in MR measurement of tissue blood flow with intravascular tracers: Which mean transit time? *Magn Reson Med* 1993; 29: 553-558.
71. Perthen JE, Calamante F, Gadian DG, et al. Is quantification of bolus tracking MRI reliable without deconvolution? *Magn Reson Med* 2002;47: 61-67.
72. Cha S, Knopp EA, Johnson G, et al. Intracranial Mass Lesions: Dynamic Contrast-enhanced Susceptibility-weighted Echo-planar Perfusion. *MR Imaging* 2002; 223: 11-29.
73. Thompson G, Mills SJ, Stivaros SM, et al. Imaging of brain tumors: Perfusion/ permeability. *Neuroimaging Clinics of North America* 2010; 20: 337-353.
74. Caseiras GB, Thornton JS, Yousry T, et al. Inclusion or Exclusion of Intratumoral Vessels in Relative Cerebral Blood Volume Characterization in Low-Grade Gliomas: Does It Make a Difference? *AJNR AM J Neuroradiol* 2008; 29: 1140-1141.
75. Wetzel SG, Cha S, Johnson G, et al. Relative Cerebral Blood Volume Measurements in Intracranial Mass Lesions: Interobserver and Intraobserver Reproducibility Study. *Radiology* 2002; 224(3): 797-803.
76. Yankeelov TE, Pickens DR, Price RR. Quantitative MRI in Cancer. Taylor & Francis. 2011. pp 224-385
77. Emblem KE, Nedregaard B, Nome T, et al. Glioma grading by using histogram analysis of blood volume heterogeneity from MR-derived cerebral blood volume maps. *Radiology. Radiological Society of North America* 2008; 247: 808-817.
78. Baek HJ, Kim HS, Kim N, et al. Percent change of perfusion skewness and kurtosis: A potential imaging biomarker for early treatment response in patients with newly diagnosed glioblastomas. *Radiology* 2012; 264: 834-843.
79. Kim HS, Kim J-H, Kim S-H, et al. Posttreatment high-grade glioma: usefulness of peak height position with semiquantitative MR perfusion histogram analysis in an entire contrast-enhanced lesion for predicting volume fraction of recurrence. *Radiology* 2010; 256: 906-915.
80. Kim H, Choi SH, Kim J-H, et al. Gliomas: Application of cumulative histogram analysis of normalized cer-

ebral blood volume on 3 T MRI to tumor grading. *PLoS ONE* 2013; 8: e63462.
81. Law M, Young R, Babb J, et al. Histogram analysis *vs* region of interest analysis of dynamic susceptibility contrast perfusion MR imaging data in the grading of cerebral gliomas. *AJNR Am J Neuroradiol* 2007; 28: 761-766.
82. Lee J, Choi SH, Kim J-H, et al. Glioma grading using apparent diffusion coefficient map: Application of histogram analysis based on automatic segmentation. *NMR Biomed* 2014; 27: 1046-1052.
83. Young R, Babb J, Law M, et al. Comparison of region-of-interest analysis with three different histogram analysis methods in the determination of perfusion metrics in patients with brain gliomas. *J Magn Reson Imaging* 2007;26: 1053-1063.
84. Bleeker EJW, van Osch MJP, Connelly A, et al. New criterion to aid manual and automatic selection of the arterial input function in dynamic susceptibility contrast MRI. *Magn Reson Med* 2011;65: 448-456.
85. Mlynash M, Eyngorn I, Bammer R, et al. Automated method for generating the arterial input function on perfusion-weighted MR imaging: Validation in patients with stroke. *AJNR Am J Neuroradiol* 2005; 26: 1479-1486.
86. Christensen S, Gyldensted L, Østergaard L. Automatic selection of arterial input function using cluster analysis. *Magn Reson Med* 2006; 55: 524-531.
87. Yin J, Sun H, Yang J. Automated detection of the arterial input function using normalized cut clustering to determine cerebral perfusion by dynamic susceptibility contrast-magnetic resonance imaging. *J Magn Reson Imaging* 2014.
88. Calamante F, Mørup M, Hansen LK. Defining a local arterial input function for perfusion MRI using independent component analysis. *Magn Reson Med* 2004; 52: 789-797.
89. Sourbron S. Technical aspects of MR perfusion. *European Journal of Radiology* 2010; 76: 304-313.
90. Vonken EJPA, van Osch MJP, Bakker CJG, et al. Simultaneous quantitative cerebral perfusion and Gd-DTPA extravasation measurement with dual-echo dynamic susceptibility contrast MRI. *Magn Reson Med* 2000; 43: 820-827.
91. Haselhorst R, Kappos L, Bilecen D, et al. Dynamic susceptibility contrast MR imaging of plaque development in multiple sclerosis: Application of an extended blood-brain barrier leakage correction. *J Magn Reson Imaging* 2000;11: 495-505.
92. Sorensen A, Reimer P. Cerebral MR perfusion imaging: Principles and current applications. Stuttgart: Thieme, 2000: 152.
93. Bjornerud A, Sorensen AG, Emblem KE. T1- and T2*-dominant extravasation correct ion in DSC-MRI: Part I - theoretical considerations and implications for assessment of tumor hemodynamic properties. *J Cereb Blood Flow Metab. Nature Publishing Group.* 2011; 31: 2041-2053.
94. Emblem KE, Bjornerud A, Borra RJH,et al. T1- and T2*-dominant extravasation correction in DSC-MRI: Part II-predicting patient outcome after a single dose of cediranib in recurrent glioblastoma patients. *J Cereb Blood Flow Metab* 2011; 31: 2054-2064.
95. Paulson ES, Schmainda KM. Comparison of dynamic susceptibility-weighted contrast-enhanced MR methods: recommendations for measuring relative cerebral blood volume in brain tumors. *Radiology* 2008; 249: 601-613.
96. Boxerman JL, Prah DE, Paulson ES, et al. The Role of preload and leakage correction in gadolinium-based cerebral blood volume estimation determined by comparison with MION as a criterion standard. *AJNR Am J Neuroradiol* 2012; 33: 1081-1087.
97. Quarles CC, Ward BD, Schmainda KM. Improving the reliability of obtaining tumor hemodynamic parameters in the presence of contrast agent extravasation. *Magn Reson Med* 2005;53: 1307-1316.
98. Knopp EA, Cha S, Johnson G, et al. Glial neoplasms: Dynamic contrast-enhanced T2*-weighted MR imaging. *Radiology* 1999; 211: 791-798.
99. Uematsu H, Maeda M, Sadato N, et al. Blood volume of gliomas determined by double-echo dynamic perfusion-weighted MR imaging: A preliminary study. *AJNR Am J Neuroradiol* 2001; 22: 1915-1919.
100. Donahue KM, Krouwer HGJ, Rand SD, et al. Utility of simultaneously acquired gradient-echo and spin-echo cerebral blood volume and morphology maps in brain tumor patients. *Magn Reson Med.* 2000; 43: 845-853.
101. Schmainda KM, Rand SD, Joseph AM, et al. Characterization of a first-pass gradient-echo spin-echo method to predict brain tumor grade and angiogenesis. *AJNR Am J Neuroradiol* 2004; 25: 1524-1532.
102. Simonsen CZ, Ostergaard L, Vestergaard-Poulsen

P, Røhl L, et al. CBF and CBV measurements by USPIO bolus tracking: reproducibility and comparison with Gd-based values. *J Magn Reson Imaging* 1999; 9: 342-347.

103. Gahramanov S, Muldoon LL, Li X, et al. Improved perfusion MR imaging assessment of intracerebral tumor blood volume and antiangiogenic therapy efficacy in a rat model with ferumoxytol. *Radiology* 2011; 261: 796-804.
104. Benner T, Heiland S, Erb G, et al. Accuracy of gamma-variate fits to concentration-time curves from dynamic susceptibility-contrast enhanced MRI: influence of time resolution, maximal signal drop and signal-to-noise. *Magnetic Resonance Imaging* 1997; 15: 307-317.
105. Lee SJ, Kim JH, Kim YM, et al. Perfusion MR imaging in gliomas: comparison with histologic tumor grade. *Korean J Radiol* 2001; 2: 1-7.
106. Law M, Yang S, Babb JS, et al. Comparison of cerebral blood volume and vascular permeability from dynamic susceptibility contrast-enhanced perfusion MR imaging with glioma grade. *AJNR Am J Neuroradiol* 2004; 25: 746-755.
107. Wong JC, Provenzale JM, Petrella JR. Pictorial essay - Perfusion MR imaging of brain neoplasms. *American Journal of Roentgenology* 2000; 174: 1147-1157.
108. Cha S, Pierce S, Knopp EA, et al. Dynamic contrast-enhanced T2*-weighted MR imaging of tumefactive demyelinating lesions. *AJNR Am J Neuroradiol* 2001; 22: 1109-1116.
109. Pollock JM, Tan H, Kraft RA, et al. Arterial spin-labeled MR perfusion imaging: Clinical applications. Magnetic Resonance Imaging Clinics of North America. 2009; 17: 315-338.
110. Sadowski EA, Bennett LK, Chan MR, et al. Nephrogenic systemic fibrosis: Risk factors and incidence estimation. *Radiology* 2007; 243: 148-157.
111. Daumas-Duport C, Scheithauer B, O'Fallon J, et al. Grading of astrocytomas. A simple and reproducible method. *Cancer* 1988; 62: 2152-2165.
112. Brem S. The role of vascular proliferation in the growth of brain tumors. *Clin Neurosurg* 1976; 23: 440-453.
113. Zagzag D, Friedlander DR, Dosik J, et al. Tenascin-C expression by angiogenic vessels in human astrocytomas and by human brain endothelial cells in vitro. *Cancer Res* 1996; 56: 182-189.
114. Aronen HJ, Gazit IE, Louis DN, et al. Cerebral blood volume maps of gliomas: comparison with tumor grade and histologic findings. *Radiology* 1994; 191: 41-51.
115. Cha S, Tihan T, Crawford F, et al. Differentiation of low-grade oligodendrogliomas from low-grade astrocytomas by using quantitative blood-volume measurements derived from dynamic susceptibility contrast-enhanced MR imaging. *AJNR Am J Neuroradiol* 2005; 26: 266-273.
116. Maia ACM, Malheiros SMF, da Rocha AJ, et al. MR cerebral blood volume maps correlated with vascular endothelial growth factor expression and tumor grade in nonenhancing gliomas. *AJNR Am J Neuroradiol* 2005; 26: 777-783.
117. Scott JN, Brasher PMA, Sevick RJ, et al. How often are nonenhancing supratentorial gliomas malignant? A population study. *Neurology* 2002; 59: 947-949.
118. Morita N, Wang S, Chawla S, et al. Dynamic susceptibility contrast perfusion weighted imaging in grading of nonenhancing astrocytomas. *J Magn Reson Imaging* 2010; 32: 803-808.
119. Law M, Oh S, Johnson G, et al. Perfusion Magnetic Resonance Imaging Predicts Patient Outcome as an Adjunct to Histopathology: A Second Reference Standard in the Surgical and Nonsurgical Treatment of Low-grade Gliomas. *Neurosurgery* 2006; 58: 1099-1107.
120. Sugahara T, Korogi Y, Kochi M, et al. Correlation of MR imaging-determined cerebral blood volume maps with histologic and angiographic determination of vascularity of gliomas. *American Journal of Roentgenology* 1998; 171: 1479-1486.
121. Shin JH, Lee HK, Kwun BD, et al. Using relative cerebral blood flow and volume to evaluate the histopathologic grade of cerebral gliomas: Preliminary results. *American Journal of Roentgenology* 2002; 179: 783i789.
122. Hakyemez B, Erdogan C, Ercan I, et al. High-grade and low-grade gliomas: Differentiation by using perfusion MR imaging. *Clin Radiol* 2005; 60: 493-502.
123. Bai X, Zhang Y, Liu Y, et al. Grading of supratentorial astrocytic tumors by using the difference of ADC value. *Neuroradiology* 2011; 53: 533-539.
124. Cho SK, Na DG, Ryoo JW, et al. Perfusion MR imaging: clinical utility for the differential diagnosis of various brain tumors. *Korean J Radiol* 2002;3: 171-179.

125. Saito T, Yamasaki F, Kajiwara Y, et al. Role of perfusion-weighted imaging at 3T in the histopathological differentiation between astrocytic and oligodendroglial tumors. *European Journal of Radiology* 2012; 81: 1863-1869.
126. Arvinda HR, Kesavadas C, Sarma PS, et al. Glioma grading: sensitivity, specificity, positive and negative predictive values of diffusion and perfusion imaging. *J Neurooncol* 2009 ;94: 87-96.
127. Scarabino T, Popolizio T, Trojsi F, et al. Ruolo delle nuove ed avanzate modalità di studio RM nella diagnostica neuroradiologica dei gliomi cerebrali. *Radiol med* 2008; 114: 448-460.
128. Lev MH, Ozsunar Y, Henson JW, et al. Glial tumor grading and outcome prediction using dynamic spin-echo MR susceptibility mapping compared with conventional contrast-enhanced MR: confounding effect of elevated rCBV of oligodendrogliomas. *AJNR Am J Neuroradiol* 2004; 25: 214-221.
129. Weber MA, Zoubaa S, Schlieter M, et al. Diagnostic performance of spectroscopic and perfusion MRI for distinction of brain tumors. *Neurology* 2006; 66: 1899-1906.
130. Danchaivijitr N, Waldman AD, Tozer DJ, et al. Low-Grade Gliomas: Do Changes in rCBV Measurements at Longitudinal Perfusion-weighted MR Imaging Predict Malignant Transformation? *Radiology* 2008; 247: 170-178.
131. Kelly PJ, Daumas-Duport C, Scheithauer BW, et al. Stereotactic histologic correlations of computed tomography- and magnetic resonance imaging-defined abnormalities in patients with glial neoplasms. *Mayo Clin Proc* 1987; 62: 450-459.
132. Hakyemez B, Erdogan C, Bolca N, et al. Evaluation of different cerebral mass lesions by perfusion-weighted MR imaging. *J Magn Reson Imaging* 2006; 24: 817-824.
133. Awasthi R, Verma SK, Haris M, et al. Comparative evaluation of dynamic contrast-enhanced perfusion with diffusion tensor imaging metrics in assessment of corticospinal tract infiltration in malignant glioma. *J Comput Assist Tomogr* 2010; 34: 82-88.
134. Law M, Cha S, Knopp EA, et al. High-Grade Gliomas and Solitary Metastases: Differentiation by Using Perfusion and Proton Spectroscopic. *MR Imaging* 2002; 222: 715-721.
135. Floriano VH, Ferraz-Filho J, Spotti AR, et al. Perfusion-weighted magnetic resonance imaging in the evaluation of focal neoplastic and infectious brain lesions. *Rev Bras Neurol* 2010.
136. Koeller KK, Rushing EJ. From the Archives of the AFIP: Oligodendroglioma and Its Variants: Radiologic-Pathologic Correlation. *Radiographics* 2005; 25: 1669-1688.
137. Whitmore RG, Krejza J, Kapoor GS, et al. Prediction of oligodendroglial tumor subtype and grade using perfusion weighted magnetic resonance imaging. *J Neurosurg* 2007; 107: 600-609.
138. Giang DW, Poduri KR, Eskin TA, et al. Multiple sclerosis masquerading as a mass lesion. *Neuroradiology* 1992; 34: 150-154.
139. Gerstner ER, Batchelor TT. Imaging and response criteria in gliomas. *Current Opinion in Oncology* 2010; 22: 598-603.
140. Bisdas S, Kirkpatrick M, Giglio P, et al. Cerebral blood volume measurements by perfusion-weighted MR imaging in gliomas: ready for prime time in predicting short-term outcome and recurrent disease? *AJNR Am J Neuroradiol. American Society of Neuroradiology* 2009; 30: 681-688.
141. Law M, Oh S, Babb JS, et al. Low-grade gliomas: Dynamic susceptibility-weighted contrast-enhanced perfusion MR imaging-prediction of patient clinical response. *Neuroradiology* 2006; 238: 658-667.
142. Law M, Young RJ, Babb JS, et al. Gliomas: Predicting time to progression or survival with cerebral blood volume measurements at dynamic susceptibility-weighted contrast-enhanced perfusion MR imaging. *Radiology* 2008;247: 490-498.
143. Caseiras GB, Chheang S, Babb J, et al. Relative cerebral blood volume measurements of low-grade gliomas predict patient outcome in a multi-institution setting. 2010;73: 215-220.
144. Romano A, Rossi Espagnet MC, Calabria LF, et al. Impiego clinico della sequenza RM di perfusione con tecnica dinamica contrastografica nei tumori cerebrali. *Radiol med* 2011; 117: 445-460.
145. Mangla R, Ginat DT, Kamalian S, et al. Correlation between progression free survival and dynamic susceptibility contrast MRI perfusion in WHO grade III glioma subtypes. *J Neurooncol* 2014; 116: 325-331.
146. Jiang Z, Le Bas J-F, Grand S, et al. Prognostic value of perfusion MR imaging in patients with oligodendroglioma: A survival study. *J Neuroradiol* 2011; 38: 53-61.

147. Maxwell RE, Long DM, French LA. The clinical effects of a synthetic gluco-corticoid used for brain edema in the practice of neurosurgery. *Steroids and Brain Edema* 1972.
148. Meinig G, Reulen HJ, Wende S. Use of Dexamethasone and Frusemide in Brain Edema Resulting from Brain Tumors. *Treatment of Cerebral* 1982.
149. Reulen HJ, Hadjidimos A, Schürmann K. The effect of dexamethasone on water and electrolyte content and on rCBF in perifocal brain edema in man. *Steroids and Brain Edema*. 1972.
150. Bastin ME, Carpenter TK, Armitage PA, et al. Effects of dexamethasone on cerebral perfusion and water diffusion in patients with high-grade glioma. *AJNR Am J Neuroradiol. American Society of Neuroradiology.* 2006;27: 402-408.
151. Andersen C, Jensen FT. Differences in blood-tumour-barrier leakage of human intracranial tumours: quantitative monitoring of vasogenic oedema and its response to glucocorticoid treatment. *Acta Neurochir (Wien)* 1998.
152. Badruddoja MA, Krouwer HGJ, Rand SD, et al. Antiangiogenic effects of dexamethasone in 9L gliosarcoma assessed by MRI cerebral blood volume maps. *Neuro-Oncology* 2003; 5: 235-243.
153. Quarles CC, Krouwer HGJ, Rand SD, et al. Dexamethasone Normalizes Brain Tumor Hemodynamics as Indicated by Dynamic Susceptibility Contrast MRI Perfusion Parameters. *Technol Cancer Res Treat* 2005; 4: 245-249.
154. Wilkinson ID, Jellineck DA, Levy D, et al. Dexamethasone and enhancing solitary cerebral mass lesions: alterations in perfusion and blood-tumor barrier kinetics shown by magnetic resonance imaging. *Neurosurgery* 2006; 58: 640-646.
155. Østergaard L, Hochberg FH, Rabinov JD, et al. Early changes measured by magnetic resonance imaging in cerebral blood flow, blood volume, and blood-brain barrier permeability following dexamethasone treatment in patients with brain tumors. J Neurosurg. *Journal of Neurosurgery Publishing Group.* 1999; 90: 300-305.
156. Stupp R, Mason WP, van den Bent MJ, et al. Radiotherapy plus concomitant and adjuvant temozolomide for glioblastoma. *N Engl J Med.* 2005; 352: 987-996.
157. Brandsma D, Stalpers L, Taal W, et al. Clinical features, mechanisms, and management of pseudoprogression in malignant gliomas. 2008;9: 453-461.
158. De Wit M, de Bruin HG, Eijkenboom W,et al. Immediate post-radiotherapy changes in malignant glioma can mimic tumor progression. *Neurology* 2004.
159. Brandes AA, Franceschi E, Tosoni A, et al. MGMT promoter methylation status can predict the incidence and outcome of pseudoprogression after concomitant radiochemotherapy in newly diagnosed glioblastoma patients. *J Clin Oncol* 2008; 26: 2192-2197.
160. Wen PY, Macdonald DR, Reardon DA, et al. Updated Response Assessment Criteria for High-Grade Gliomas: Response Assessment in Neuro-Oncology Working Group. *Journal of Clinical Oncology* 2010; 28: 1963-1972.
161. Tsien C, Galban CJ, Chenevert TL, et al. Parametric Response Map As an Imaging Biomarker to Distinguish Progression From Pseudoprogression in High-Grade Glioma. *Journal of Clinical Oncology* 2010; 28: 2293-2299.
162. Kong DS, Kim ST, Kim EH, et al. Diagnostic dilemma of pseudoprogression in the treatment of newly diagnosed glioblastomas: the role of assessing relative cerebral blood flow volume and oxygen-6-methylguanine-DNA methyltransferase promoter methylation status. AJNR Am J Neuroradiol. *American Society of Neuroradiology* 2011; 32: 382-387.
163. Young RJ, Gupta A, Shah AD, et al. MRI perfusion in determining pseudoprogression in patients with glioblastoma. *Clinical Imaging* 2013; 37: 41-49.
164. Gahramanov S, Muldoon LL, Varallyay CG, et al. Pseudoprogression of Glioblastoma after Chemo- and Radiation Therapy: Diagnosis by Using Dynamic Susceptibility-weighted Contrast-enhanced Perfusion MR Imaging with Ferumoxytol versus Gadoteridol and Correlation with Survival. 2013; 266: 842-852.
165. Friedman HS, Schold SC, Djang WT, et al. Criteria for termination of phase II chemotherapy for patients with progressive or recurrent brain tumor. *Neurology* 1989.
166. Chang SM, Prados MD. Chemotherapy for gliomas. *Current Opinion in Oncology* 1995.
167. Verhoef C, de Wilt JHW, de Wilt J, et al. Angiogenesis Inhibitors: Perspectives for Medical, Surgical and Radiation Oncology. CPD. 2006;12: 2623-2630.
168. Gossmann A, Helbich TH, Kuriyama N, et al. Dynamic contrast-enhanced magnetic resonance imaging as

a surrogate marker of tumor response to anti-angiogenic therapy in a xenograft model of glioblastoma multiforme. *J Magn Reson Imaging* 2002; 15: 233-240.

169. Leach MO, Brindle KM, Evelhoch JL, et al. The assessment of antiangiogenic and antivascular therapies in early-stage clinical trials using magnetic resonance imaging: issues and recommendations. *Br J Cancer* 2005; 92: 1599-1610.
170. Sawlani RN, Raizer J, Horowitz SW, et al. Glioblastoma: A Method for Predicting Response to Antiangiogenic Chemotherapy by Using MR Perfusion Imaging-Pilot Study. 2010; 255: 622-628.
171. Essock-Burns E, Lupo JM, Cha S, et al. Assessment of perfusion MRI-derived parameters in evaluating and predicting response to antiangiogenic therapy in patients with newly diagnosed glioblastoma. *Neuro-Oncology* 2011; 13: 119-131.
172. Batchelor TT, Gerstner ER, Emblem KE, et al. Improved tumor oxygenation and survival in glioblastoma patients who show increased blood perfusion after cediranib and chemoradiation. *Proc Natl Acad Sci USA. National Academy of Sciences* 2013; 110: 19059-19064.
173. Cha S, Knopp EA, Johnson G, et al. Dynamic contrast-enhanced T2-weighted MR imaging of recurrent malignant gliomas treated with thalidomide and carboplatin. *AJNR Am J Neuroradiol* 2000; 21: 881-890.
174. van den Bent MJ, Vogelbaum MA, Wen PY, et al. End Point Assessment in Gliomas: Novel Treatments Limit Usefulness of Classical Macdonald's Criteria. *Journal of Clinical Oncology* 2009; 27: 2905-2908.
175. Gerstner ER, Sorensen AG, Jain RK, et al. Advances in neuroimaging techniques for the evaluation of tumor growth, vascular permeability, and angiogenesis in gliomas. *Current Opinion in Neurology* 2008; 21: 728-735.
176. Batchelor TT, Sorensen AG, di Tomaso E, et al. AZD2171, a Pan-VEGF Receptor Tyrosine Kinase Inhibitor, Normalizes Tumor Vasculature and Alleviates Edema in Glioblastoma Patients. *Cancer Cell* 2007; 11: 83-95.
177. Hu LS, Baxter LC, Smith KA, et al. Relative cerebral blood volume values to differentiate high-grade glioma recurrence from posttreatment radiation effect: Direct correlation between image-guided tissue histopathology and localized dynamic susceptibility-weighted contrast-enhanced perfusion. *MR imaging measurements* 2009; 30: 552-558.
178. Barajas RF Jr, Chang JS, Segal MR, et al. Differentiation of Recurrent Glioblastoma Multiforme from Radiation Necrosis after External Beam Radiation Therapy with Dynamic Susceptibility-weighted Contrast-enhanced Perfusion, *MR Imaging1* 2009; 253: 486-496.
179. Xu JL, Shi DP, Dou SW, et al. Distinction between postoperative recurrent glioma and delayed radiation injury using MR perfusion weighted imaging. *Wiley Online Library* 2011; 55: 587-594.
180. Margaret Cheng H-L. Dynamic Contrast-Enhanced MRI in Oncology Drug Development. *CCP. Bentham Science Publishers* 2007; 2: 111-122.
181. Ali MM, Janic B, Babajani-Feremi A, et al. Changes in Vascular Permeability and Expression of Different Angiogenic Factors Following Anti-Angiogenic Treatment in Rat Glioma. *PLoS ONE* 2010; 5: e8727.
182. Hygino da Cruz LC, Rodriguez I, Domingues RC, et al. Pseudoprogression and pseudoresponse: Imaging challenges in the assessment of posttreatment glioma. *American Society of Neuroradiology* 2011; 32: 1978-1985.
183. Ellingson BM, Kim HJ, Woodworth DC, et al. Recurrent Glioblastoma Treated with Bevacizumab: Contrast-enhanced T1-weighted Subtraction Maps Improve Tumor Delineation and Aid Prediction of Survival in a Multicenter Clinical Trial. *Radiology. Radiological Society of North America.* 2013; 271: 200-210.
184. Lupo JM, Nelson SJ. Advanced magnetic resonance imaging methods for planning and monitoring radiation therapy in patients with high-grade glioma. Seminars in Radiation. *Oncology*2014; 24: 248-258.
185. Qiao XJ, Ellingson BM, Kim HJ, et al. Arterial Spin-Labeling Perfusion MRI Stratifies Progression-Free Survival and Correlates with Epidermal Growth Factor Receptor Status in Glioblastoma. *AJNR Am J Neuroradiol. American Society of Neuroradiology* 2014.
186. Schmainda KM, Zhang Z, Prah M, et al. Dynamic susceptibility contrast MRI measures of relative cerebral blood volume as a prognostic marker for overall survival in recurrent glioblastoma: Results from the ACRIN 6677/RTOG 0625 multicenter trial. *Neuro-Oncology* 2015; 364.
187. Yankeelov TE, Gore JC. Dynamic Contrast Enhanced Magnetic Resonance Imaging in Oncology: Theory,

Data Acquisition, Analysis, and Examples. *Curr Med Imaging Rev* 2009; 3: 91-107.
188. Golay X, Guenther M. Arterial spin labelling: Final steps to make it a clinical reality. *Magn Reson Mater Phy* 2012; 25: 79-82.
189. Jain R. Measurements of tumor vascular leakiness using DCE in brain tumors: clinical applications. Lu H, editor. NMR Biomed. 2013;26: 1042-1049.
190. Ellingson BM, Bendszus M, Sorensen AG, Pope WB. Emerging techniques and technologies in brain tumor imaging. *Neuro-Oncology. Oxford University Press.* 2014; 16 Suppl 7: vii12–vii23.

READY - MADE CITATION

Fallatah S, Golay X, Jäger R, Bisdas S. Dynamic Susceptibility Contrast MRI in Gliomas: What the Radiologist Needs to Know. *Hell J Radiol* 2016; 1(1): 56-78.